

## Spin–orbit effects in the formation of the Na–He excimer on the surface of He clusters

James Reho, Carlo Callegari, John Higgins, Wolfgang E. Ernst, Kevin K. Lehmann and Giacinto Scoles

Department of Chemistry, Princeton University, Princeton, New Jersey 08544, USA

---

In this paper we describe an application of reversed time-correlated single photon counting to the time-resolved spectroscopy of impurity atoms and molecules bound to large quantum clusters. The photo-induced dynamics of Na atoms on the surface of He and H<sub>2</sub> clusters have been studied by following the time dependence of their emission at selected excitation and emission wavelengths. Collection of atomic ( $16980 \pm 145 \text{ cm}^{-1}$ ) fluorescence arising from Na atoms excited on the cluster surface and immediately desorbed from it yields a finite (*ca.* 70 ps) rise time and a decay time of  $16.3 \pm 0.1 \text{ ns}$ , equal to the known lifetime of the  $3P \rightarrow 3S$  transition of atomic Na. The frequency distribution of the red emission due to atoms that do not leave the cluster immediately after excitation is shown to be due to a desorbed Na\*–He exciplex by obtaining quantitative agreement with predictions derived from available *ab initio* Na–He potentials. Formation of this excimer can occur along either the  $^2\Pi_{1/2}$  or  $^2\Pi_{3/2}$  excited state surface. ‘Slow’ (700 ps) and ‘fast’ (*ca.* 70 ps) components of the rise time of the red emission ( $15800 \pm 125 \text{ cm}^{-1}$ ) are assigned, respectively, to the two formation channels. Introducing spin–orbit coupling effects into the long range *ab initio* pair potential for an isolated Na\*–He generates a small barrier on the  $^2\Pi_{1/2}$  potential curve, which is linked to the observed slow exciplex formation time.

---

### Introduction

Extensive experimental and theoretical work has probed the interaction of atoms and molecules seeded in bulk liquid helium and in or on large helium clusters.<sup>1–11</sup> Although many atomic dopants have been studied,<sup>1</sup> alkali-metal atoms have come to play a crucial role due to their simple electronic configuration which makes it feasible to probe and model changes in helium morphology as the dopant undergoes optical excitation. Neutral alkali-metal atoms have been introduced into bulk liquid He by laser sputtering techniques<sup>2</sup> and have been probed by optical means. The optical excitation and emission of alkali-metal atoms (Cs and Rb) in bulk liquid helium show substantial shifts and broadening in spectral regions corresponding to the D lines of the free atoms. The spectra obtained in the region of the D<sub>1</sub> atomic lines of Cs and Rb can be simulated within the framework of the bubble model<sup>3</sup> in which the Pauli repulsion between the helium bath and the alkali-metal atoms produces a spherical cavity inside the He. Additionally, magnetic resonance signals arising from optically pumped, optically detected Cs and Rb trapped in bulk He likewise have been reproduced using the bubble model.<sup>4</sup> However, the doubly shaped profiles of the D<sub>2</sub> excitation spectra of Cs in the bulk cannot be predicted using a simple spherical bubble and have been attributed to deformation of the bubble by a quadrupole oscillation.<sup>5</sup> In the refinement of the bubble

model, spherical symmetry of the helium cavity (and hence the degeneracy of the excited atomic p states) is removed by a dynamic Jahn–Teller effect. Analogously, Kanorsky *et al.*<sup>6</sup> postulate a deformation of the bubble after electronic excitation of atomic Na in bulk liquid He. Describing the Na atom in terms of one-electron orbitals, they suggest that a few (from four to six) He atoms ‘flow’ into the ‘waist’ of the  $p_z$  wavefunction, taking advantage of the relative lack of repulsion in the area of the  $p_z$  nodal plane. When the number of helium atoms on the  $p_z$  nodal plane of Na is increased to five, the 3S and 3P atomic Na levels are practically degenerate and radiationless transitions to the atomic ground state from both D lines become possible.<sup>7</sup> This model has been proposed as an explanation for the absence of fluorescence from optically excited Na and Li in bulk liquid helium.

For larger alkali-metal atoms (Cs, Rb), the accessibility of this non-radiative decay channel depends upon which of the two fine structure sublevels of the P state ( $P_{1/2}$  or  $P_{3/2}$ ) is excited. According to Yabuzaki and coworkers,<sup>8</sup> the quenching of  $P_{1/2} \rightarrow S_{1/2}$  fluorescence seen in Rb occurs owing to several He atoms closely approaching the alkali-metal atomic core which opens a non-radiative decay channel, paralleling the predictions for lighter atoms stated above.

Mechanisms also exist which account for reduced  $P_{3/2} \rightarrow S_{1/2}$  alkali-metal fluorescence in bulk He. One involves the rapid population transfer from the  $P_{3/2}$  state down to the  $P_{1/2}$  level, which becomes possible as the He bath allows for L–S uncoupling. Under the perturbation of the surrounding liquid, L–S coupling is preserved in the case of Cs (large fine structure), while for Rb it is thought to be partially broken. The non-statistical ratios of the  $P_{1/2}$  and  $P_{3/2}$  line intensities of Cs and Rb<sup>5</sup> support the presence of this depopulation mechanism. Experimental evidence also points to an additional non-radiative decay channel from the  $P_{3/2}$  state which at present remains uncharacterized.<sup>8</sup>

When a helium cluster beam picks up an alkali-metal atom, the latter is predicted to reside on the surface of the cluster owing to the predominantly repulsive nature of the interaction of the alkali-metal atom with helium. Indeed, because of the large size of the Na atom and the  $1/r^6$  dependence of dispersion forces, the attractive part of the Na–He pair potential is calculated to be much weaker than the self-interaction of helium.<sup>9</sup> The surface site occupied by the Na in the case of the cluster changes the dynamic picture of the atomic interaction with the substrate. The atom is postulated to sit above a ‘dimple’ formed on the helium surface owing to the alkali-metal–He repulsion<sup>9</sup> and to be farther removed from the helium than is the case in the bulk. Experimental work in our laboratory has confirmed this prediction of location on a surface site while probing both bound–bound and bound–free transitions of the atom–cluster complex.<sup>10</sup> The simple fact that in our case the  $D_1$  and  $D_2$  lines of Na and K on the He cluster are of roughly equal intensity<sup>10</sup> stands in contrast to the findings in the bulk noted above in which the proximity of the helium aids in a depletion of the  $J = 3/2$  population into the lower ( $J = 1/2$ ) atomic P spin–orbit level. Additionally, fluorescence from Li atoms on He clusters has been observed,<sup>10</sup> while it appears that in the bulk the  $2P_{3/2, 1/2} \rightarrow 2S_{1/2}$  fluorescent decay channel of atomic Li and Na is fully quenched by non-radiative processes.

While a reasonably clear picture of the alkali-metal/cluster interaction has emerged from our work,<sup>10</sup> the dynamical behavior of the system is not yet fully understood. In particular, we have not yet resolved the molecular processes that may occur on the cluster surface, such as the vibrational cooling of excited dimers and the photo-dissociation of trimers. This is why we have assembled a reversed time-correlated single photon counting apparatus which allows us to obtain time-resolved spectra with a time resolution on the order of 20 ps. As a first application of this instrument, we have studied the photoinduced dynamics of Na atoms on the surface of helium and hydrogen clusters by following the time dependence of their emission at selected excitation and

emission wavelengths. It is hoped that by time-resolving the dynamics on the cluster surface we can also obtain information that could be useful in explaining some aspects of the studies conducted in the bulk that depend on the response time of the matrix in adapting itself to the changes induced by the electronic excitation of the ‘impurities’.

Before describing the time-resolved studies, we will briefly review the excitation spectra of alkali-metal atoms (Li, Na, K) on the surface of helium clusters performed in our laboratory, as this work provides the framework for the present experiments. These excitation spectra exhibit intensities at, and slightly to the red of, the corresponding free atomic D lines, in conjunction with a long tail extending to the blue. Successful modelling requires both bound–bound and bound–free transitions on a cluster/alkali-metal pseudodiatomic potential surface. The dispersed fluorescence of the  $3^2P_{1/2, 3/2} \leftarrow 3^2S_{1/2}$  atomic transitions of Na atoms on the cluster surface exhibits intensities at both the free atom transitions and at substantially red-shifted frequencies. While the free atom fluorescence is due to rapid atomic desorption from the cluster by the electronic excitation, we assign the red-shifted emission to the formation of some alkali-metal/helium complex, as discussed in detail below. This finding parallels the results found in the bulk by the group of Takami<sup>11</sup> in which the AgHe<sub>2</sub> excimer was found to form from the optically excited atom in a bath of liquid helium. Below we show that helium cluster isolation spectroscopy, coupled with our photon counting system, allows us to gain direct insight into the dynamics of the Na\*–He excimer formation.

## Experimental

Only a brief description of the methodology used for the production of alkali-metal doped He clusters in our laboratory will be presented here, as a more detailed explanation has been given elsewhere.<sup>10</sup> On the other hand, a full description of our apparatus for time resolved laser spectroscopy of doped He clusters, never having been previously reported, is given below.

A beam of large He nanodroplets ( $\langle N \rangle \approx 10^3$ – $10^4$ ) is produced in a free jet expansion of He gas using a stagnation pressure of 5.4 MPa, a nozzle temperature of 17.5 K, and a nozzle diameter of 20  $\mu\text{m}$ . After collimation by a 400  $\mu\text{m}$  diameter skimmer, the clusters are doped with sodium atoms using the pick-up technique<sup>12</sup> by passing the He cluster beam through a cell containing a pressure of *ca.*  $10^{-2}$  Pa of sodium. The doped clusters can be probed spectroscopically by laser induced fluorescence (see below) and by laser induced beam depletion of the signal produced by a hot wire detector when the Na atoms carried by the clusters are ionized on its surface.

The apparatus used in the time-resolved studies is shown schematically in Fig. 1. A mode-locked, frequency-doubled YAG laser (Quantronix 416) synchronously pumps a folded-cavity dye laser (Spectra Physics 3500), producing pulses of 10–12 ps full width at half maximum (FWHM) as determined by autocorrelation. The linewidth of the laser is  $2 \text{ cm}^{-1}$ , which is twice the Fourier transform limit. Given the 16 ns radiative lifetime of the sodium  $3^2P_{1/2, 3/2}$  state, use of the dye laser’s 75.7 MHz repetition rate (*i.e.*, a 13.2 ns interval between pulses) leads to substantial overlap of the emission from several excitation pulses. A home-built ‘pulse-picker’ is used to enlarge the pulse period to 85.2 ns which is the period used in the present experiments.

Laser induced fluorescence of the Na-doped He clusters is collected by a high efficiency double mirror optic and transported to a microchannel plate detector (MCD; Hamamatsu R2807U-07) through a multimode, incoherent fiber bundle. In order to allow for wavelength selection, band pass filters are introduced in front of the microchannel plates. Lifetime measurements use the reversed time-correlated single photon counting technique. The fluorescence signal from the MCD is amplified (two Mini-circuits ZFL-2000 preamplifiers are used) and passes through a constant fraction discriminator (Tennelec TC454) which provides the start signal of a time-to-amplitude

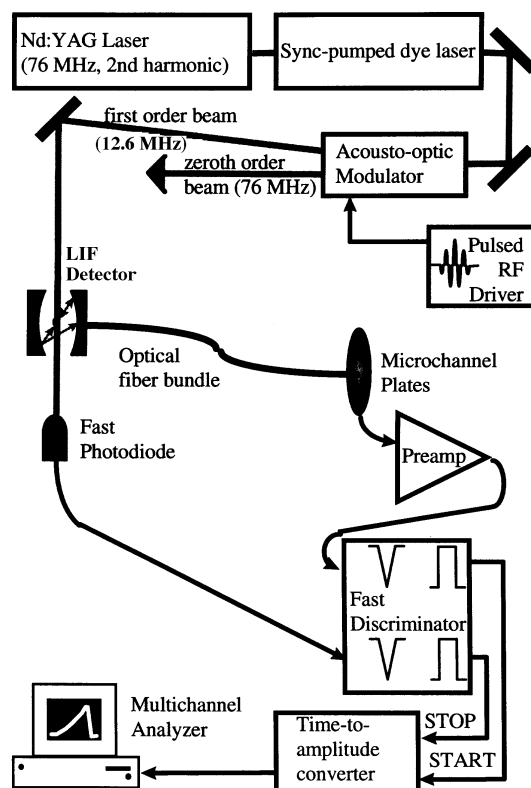


Fig. 1 Apparatus for time-correlated single photon counting

converter (TAC; Ortec 457). The laser pulse that triggers the fluorescent event is detected by a fast photodiode, amplified and appropriately delayed, and processed by a constant fraction discriminator. This signal is then used as the stop signal in the TAC. This 'reverse' method insures that the each 'start' pulse is followed by a 'stop' pulse inside the time window of the TAC. The output of the TAC is processed by a multichannel analyzer (Nucleus II) and binned, thus compiling our experimental histograms which give the emission intensity as a function of time after each excitation pulse. The multichannel analyzer contains 8192 channels which we have set to cover a 100 ns region in time. The instrument was calibrated by a pulse generator (Stanford Research Systems) and was found to be linear over the 100 ns time window with a standard deviation of the fit of 20 ps. Count rates encountered in these experiments varied between 200 and 3000 photons per second. At these count rates, pile-up error in the TAC is avoided.<sup>13</sup>

We have measured the instrument response function by passing  $H_2$  through a 34.7 K nozzle with a 20  $\mu\text{m}$  diameter at backing pressures in excess of 300 psi. This produces a beam comprised of large frozen hydrogen particles which acts as a scatterer of our laser light probe. We thus define the histogram of this cold  $(H_2)_n$  beam scatter signal as a measure of the instrument function. A typical instrument response function is shown in Fig. 2. The response consists of two peaks, separated in time by 400 ps with a 170 ps FWHM for each peak. The separation of the two peaks matches the delay expected from photons that bounce off the spherical and elliptical mirrors compared to those that bounce only off the elliptical mirror of the fluorescence imaging system, which was designed to maximize collection efficiency, not time resolution. The observed instrument

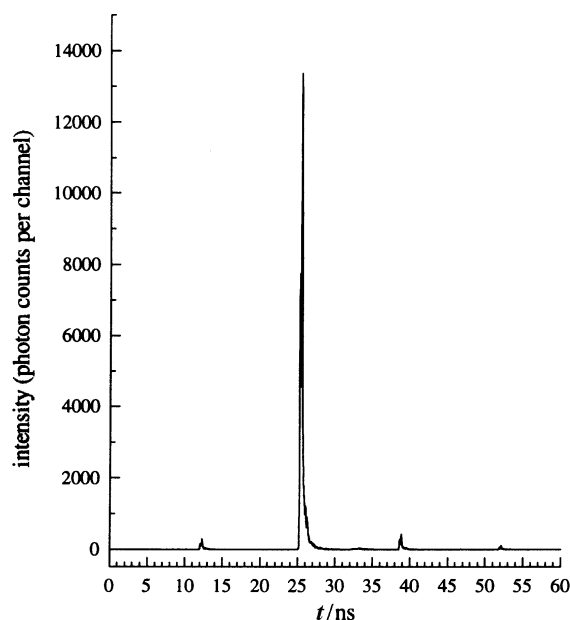


Fig. 2 Typical instrument response function obtained from the time-correlated single photon counting apparatus

response is insensitive to whether the ‘stop’ pulse arises from the same laser pulse that created the excitation (effected with the use of delay lines), or the subsequent laser pulse.

The time resolution of the instrument is determined by the initial laser pulse width and by the additional timing jitter associated with detection and subsequent electronic processing, and is presently estimated at 20 ps. The rise time (10% to 90% of full intensity) of the microchannel plate detector is 148 ps with a time jitter of less than 15 ps.<sup>14</sup> Both start and stop pulse are amplified with bandwidths of 2 GHz, leading to little pulse broadening. The rise time of the fast photodiode is 500 ps, but as this signal is much more stable in amplitude than the MCD, it is expected to have lower timing jitter. An important unknown at present is the transit time broadening caused by light passing through the multimode fiber bundle.

## Data analysis

Modelling of our data is carried out through an iterative convolution method written using the Mathcad suite of programs in which the numerical instrument function (measured by H<sub>2</sub> cluster scattering with all other experimental conditions the same as for our time-resolved experiments using He clusters) is convoluted with a kinetic model by use of a pair of Fast Fourier Transforms. The following kinetic model is used:

$$G(t) = [A \exp(-t/\tau_1) - \exp(-t/\tau_2)] + D$$

in which  $\tau_2$  and  $\tau_1$  represents the rise and fall times, respectively, of the population of the fluorescing species.  $D$  is a background factor that accounts for the dark counts in the MCD, calculated from the measured total dark count rate and the total signal averaging time for each bin. When the fit to this function is found unsatisfactory (based upon standard  $\chi^2$  analysis), a model which is biexponential in rise and fall is used:

$$G(t) = \{A[\exp(-t/\tau_1) - \exp(-t/\tau_2)] + B[\exp(-t/\tau_3) - \exp(-t/\tau_4)]\} + D$$

The amplitudes  $A$  and  $B$  as well as the exponential arguments  $\tau_i$  (*i.e.*, the rise and fall times) of the model are parameters in a weighted least squares fit to the observed fluorescence decay curve. Weights of each bin are calculated based upon Poisson statistics; a weighting factor of  $1/N_i$  is used to weight each bin, where  $N_i$  is the observed number of counts in the  $i$ th bin. The global minimum of  $\chi^2$  is sought through the Marquardt algorithm. A model is deemed successful if the reduced chi squared ( $\chi_r^2$ ) is close to unity. A typical result is a  $\chi_r^2 = 1.2$ . The standard deviations as well as correlations between model parameters<sup>15</sup> are found through standard equations based upon a linear approximation for the variation of the model with parameters. This fitting method avoids the problems of noise amplification prevalent in the deconvolution of an instrument response function from the experimental histogram by Fourier transform methods.

## Results

The excitation and dispersed emission spectra of Na atoms on He clusters were previously measured in our laboratory.<sup>10</sup> The excitation spectrum obtained by integrating over the complete emission spectrum is illustrated in Fig. 3. It is seen that the spectrum begins slightly to the red of the free Na  $3P_{1/2, 3/2} \leftarrow 3S_{1/2}$  lines and exhibits a long tail on the blue side. The dispersed emission spectra consist of two main features, the relative intensities of which change as a function of the excitation frequency. The first feature has an instrumentally limited linewidth and corresponds to the emission of gas phase Na\* (*i.e.*, the free atom D lines), while the second is a broad, structured feature with intensity spanning the range from  $14\,200\text{ cm}^{-1}$  to  $16\,800\text{ cm}^{-1}$ . In our earlier publication<sup>10</sup> the excitation spectrum was modelled by assuming that the spectrum consists of contributions from both bound-bound and bound-free transitions occurring between the ground state and first excited state of the Na-cluster potential. The atomic emission was assigned to gas phase Na\* atoms produced by the bound-free transition while a species containing Na atoms excited in bound-bound transitions was assigned as the source of the 'red' emission. This allows for an empirical way to separate the bound-bound and

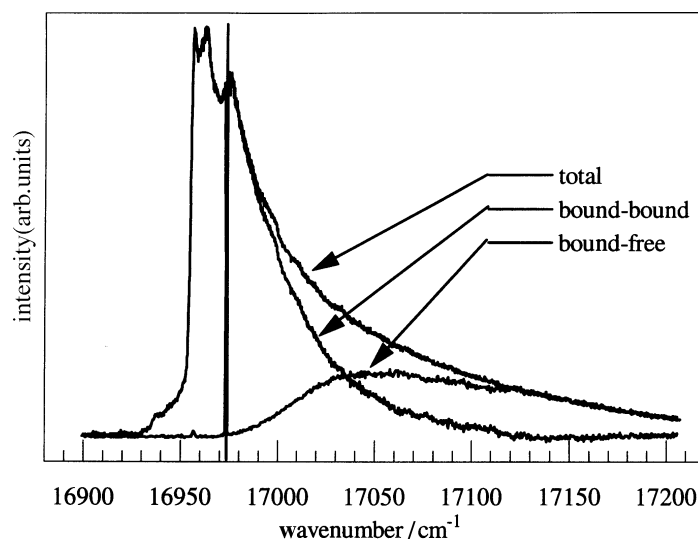


**Fig. 3** Excitation spectrum of Na atoms on He clusters illustrating how the spectrum is composed of bound-free and bound-bound contributions. The bound-free contribution is measured by monitoring fluorescent emission at the gas phase lines. The bound-bound contribution is determined by collecting red-shifted fluorescent emission

bound-free contributions to the absorption by measuring emission-wavelength-selected excitation spectra, which are also shown in Fig. 3. It can be seen that the free atom emission (bound-free excitation) does not begin until  $18 \text{ cm}^{-1}$  above the wavenumber of the  $^2\text{P}_{1/2}$  line. This provides a direct measure of the binding energy of the ground state Na atom on the cluster. It is also seen that the ‘bound-bound’ transitions extend beyond the onset of bound to free transitions by far more than the atomic spin-orbit splitting, which would not be expected if we were dealing with a rigid surface. The higher energy absorption reflects simultaneous excitation of the Na atom along with vibrational modes of the He cluster.

The observation of emission from bound-bound transitions is perhaps surprising given the well established fact that the light alkali-metal atoms do not give detectable fluorescence from bubble states in bulk liquid He. It is believed that the excited Na atom is rapidly quenched owing to the attraction of a ring of five or six He atoms around the nodal plane of the p orbital, which allows them to interact strongly with the  $\text{Na}^+$  core without excessive Pauli repulsion.<sup>7</sup> The He-Na interaction is highly repulsive in the ground state at such distances, probably resulting in a curve crossing which would lead to quenching. While one would expect the quenching to be slower for  $\text{Na}^*$  on the surface than in the bulk, the measured wavelength-selective excitation spectra suggest that the emission quantum yield of atoms leading to red emission is large thus giving no experimental evidence of quenching.

Measurements of rise and fall times were made at several points in the excitation spectrum collecting either atomic ( $16980 \pm 145 \text{ cm}^{-1}$ ) or red-shifted ( $15800 \pm 125 \text{ cm}^{-1}$ ) fluorescence. The results of these fits are presented in Table 1. We will first discuss the results of fits to decays observed at the free atom emission wavelength. These fits correspond to excitation to the blue of the atomic lines while collecting the gas phase fluorescence. The resulting decay times were centered around  $16.3 \pm 0.1 \text{ ns}$ , in excellent agreement with the well known radiative lifetime of the Na D lines,<sup>16</sup> confirming the ability of our instrument to provide accurate lifetimes. Times of 50 ps and 70 ps were found for the fluorescence rise times (*i.e.*, mean time of the onset of fluorescence) under the same conditions. These values are less than the width of the instrument function (170 ps), but larger than the factor of one-tenth FWHM of the instrument function (*ca.* 20 ps) that is often claimed as the shortest time resolvable by the time-correlated photon counting instrument.<sup>17</sup> Fits to emission from excitation of gas phase Na atoms (which should give an infinitely fast rise for the model that is convoluted with the instrument function) gave rise times of under 20 ps. For a bound-free transition, we expect the free atom emission to increase with a rise time on the order of the vibrational period of the

**Table 1** Time-resolved fluorescence rise and fall times for Na atoms on He clusters

excitation energy/ $\text{cm}^{-1}$	rise time/ps	fall time/ns
fluorescence at $16980 \pm 145 \text{ cm}^{-1}$ (free atoms)		
17041	$50 \pm 30$	$16.3 \pm 0.1$
17084	$50 \pm 30$	$16.3 \pm 0.1$
17127	$70 \pm 30$	$16.3 \pm 0.1$
17385	$70 \pm 30$	$16.2 \pm 0.1$
fluorescence at $15800 \pm 125 \text{ cm}^{-1}$ (excimers)		
16945	$700 \pm 30$	$18.2 \pm 0.1$
16956	$700 \pm 30$	$18.2 \pm 0.1$
16973	$80 \pm 30$	$20.1 \pm 0.1$
16994	$70 \pm 30$	$20.7 \pm 0.1$
17041	$80 \pm 30$	$21.2 \pm 0.1$

Na\*–cluster attractive potential. Based upon the previous estimates of this potential,<sup>10</sup> this period should be *ca.* 15 ps. However, the He cluster does not provide a rigid surface and its response times are thus difficult to predict *a priori*. In summary, at this point in time, we note that the expulsion times of the excited Na atoms from the cluster appear to be larger than our instrumental resolution but we stop short of claiming the ability to confidently resolve these times with the instrument as it stands. We are presently setting up pump and probe experiments in which rise times larger than several picoseconds should prove easily resolvable.

Collection of the red-shifted ( $15\,798 \pm 125\text{ cm}^{-1}$ ) fluorescence yielded fluorescence curves that gave rise times that depended strongly on the excitation wavelength, but fall times ranging from 19 to 21 ns, longer than the free atom value. If we assume that this decay has the same transition dipole as for the atom and take the mean emission wavelength as  $15\,798\text{ cm}^{-1}$ , we predict a radiative lifetime of 20 ns, in excellent agreement with the observed value. This implies that there is negligible quenching of this emitting species by the He cluster, in dramatic contrast to the complete quenching observed in bulk liquid <sup>4</sup>He. In former work from our laboratory<sup>10</sup> we postulated a molecule-like transition as the originator of this red fluorescence. As a result of our time-resolved observations, we were able to conclude that this red emission was due primarily to a species emitting in the gas phase as quenching (and thus a decrease in lifetime) would otherwise have been observed. As will be demonstrated below, we find that the red emission is in excellent agreement with the calculated bound-free  $3^2\text{P} \rightarrow 3^2\text{S}$  emission from an isolated Na\*–He excimer that has desorbed from the cluster. Na\*–He diatoms that do not desorb from the cluster would be expected to 'suck up' additional He atoms from the cluster, leading to emission further shifted to the red, where no emission was observed in our previous work. It thus appears that the Na\*–He exciplex has nearly unit probability to desorb from the cluster.

We now turn attention to the rise times observed when the red emission centered at  $15\,798\text{ cm}^{-1}$  is monitored. For excitation energies to the blue of the atomic  $J = 3/2$  line, the observed fluorescence is successfully fitted to a model with a single rise time, which is found to be 70 ps, only slightly longer than the rise time observed for the atomic emission. This argues that following such excitation, the formation and desorption of the Na\*–He exciplex occurs very rapidly. This suggests that the desorption is probably directly coupled to the formation process. As we move the excitation wavelength to the red of the  $J = 3/2$  atomic line, we find that to successfully fit the observed fluorescence signals, we must use two rise times. One component of the emission (the amplitude of which decreases as the excitation is moved to the red) also has a rapid rise time (70 ps). However, the second component has a much slower rise time (*ca.* 700 ps). As will be discussed below, we assign the rapid rise time to formation of the Na\*–He on the  $^2\Pi_{3/2}$  surface (which correlates with the atomic  $J = 3/2$  fine structure component) and the slow rise to formation of the Na\*–He on the  $^2\Pi_{1/2}$  surface (which correlates with the atomic  $J = 1/2$  fine structure component).

We close this section with one last observation, in which we analyze the emission following excitation of Na on large H<sub>2</sub> clusters. Previous work by our group had established that Na\* on H<sub>2</sub> clusters has a small quantum yield for emission (roughly 1%), and that all of the observed emission appears at the gas phase wavelength, suggesting that only the small fraction of molecules that desorb from the cluster escape quenching.<sup>18</sup> The overwhelming presence of quenching and the shape of the absorption spectrum of Na\* was determined (without the bias of a wavelength dependent quantum yield) by use of a Langmuir–Taylor detector which monitored depletion of Na atoms from the cluster beam. The mechanism of beam depletion in this case is as yet uncertain, and is presently thought to be due to either desorption of the Na atom from the cluster, or from spreading of the cluster beam caused by the desorption of *ca.* 300 hydrogen molecules owing to the heat liberated upon quenching of the electronic excitation. The

observed time-dependent emission is also in this case successfully fit to a model with a single free atom decay time (as expected), and a rise of 20 ps. This result suggests that the desorption comes from atoms excited to bound-free transitions from the surface of the  $H_2$  clusters. Previous theoretical calculations had predicted that Na would be solvated and reside inside large  $H_2$  clusters.<sup>9</sup> The present results demonstrate that at least a small fraction reside on the surface, and, furthermore, lend support to the possibility that the slower evaporation times measured for the excited Na atom on He clusters (50–70 ps) may be real.

## Discussion

### (a) Modelling of the frequency spectrum of the $Na^* - He \ 3^2P \rightarrow 3^2S$ emission

Potentials of both  $Na(3^2S) - He$  and  $Na(3^2P) - He$  interactions are available in the literature.<sup>19,20</sup> Experimental information on these curves is also available from studies of the red tail of the emission of  $Na^*$  in high pressure He gas.<sup>19</sup> Fig. 4 shows the potential curves as calculated by Pascale neglecting spin-orbit effects.<sup>20</sup> We see that we have a predominantly repulsive  $^2\Sigma$  state and a fairly attractive  $^2\Pi$  state correlating to the atomic  $Na(3P)$  asymptote. The ground state is of course repulsive at short range but also very weakly attractive at long range with a well depth of  $2.4 \text{ cm}^{-1}$ .

Fig. 5 shows the dispersed emission spectrum observed following excitation of Na at  $16975.2 \text{ cm}^{-1}$  in which a structure with four peaks is seen. The vertical emission from the lowest four bound states produced by the well of the  $(A)^2\Pi$  state to the repulsive

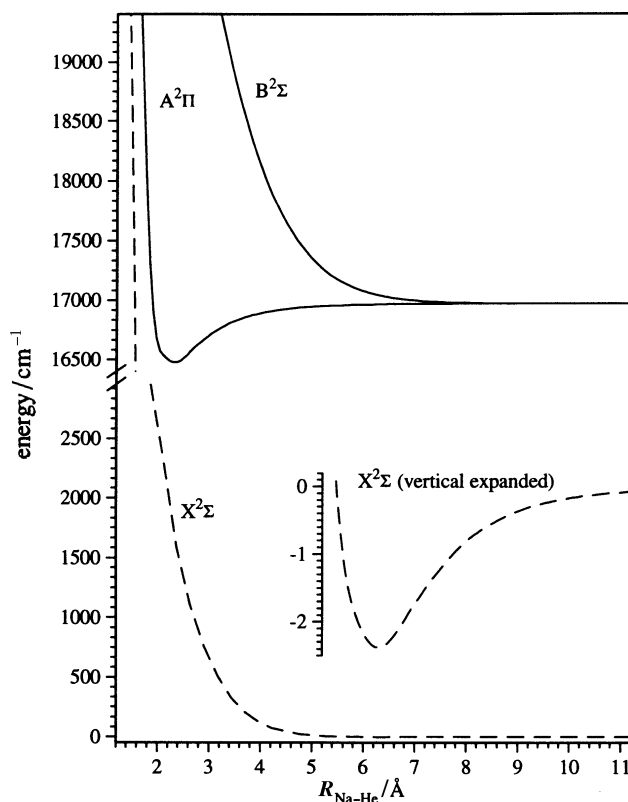
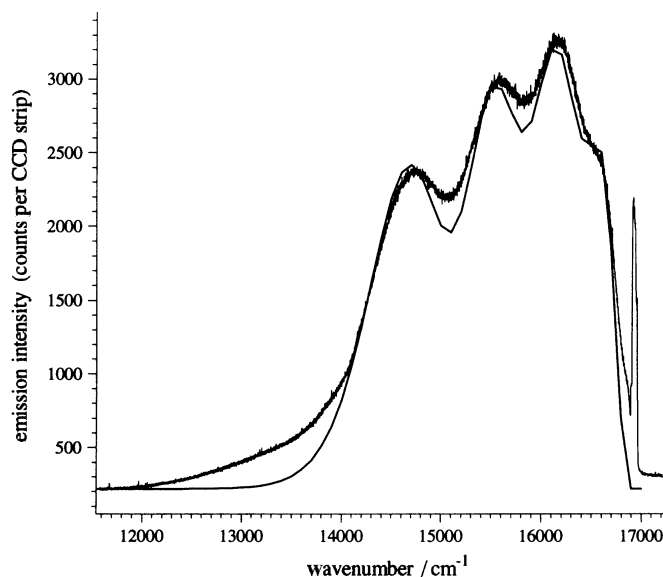


Fig. 4 Na-He potential curves as calculated by Pascale<sup>20</sup>



**Fig. 5** Dispersed fluorescence spectrum of Na\*–He excimers desorbed from He clusters after excitation of Na atoms on the surface of the cluster. The excitation energy is  $16975\text{ cm}^{-1}$ . The continuous line is a simulated emission spectrum calculated using Pascale's potentials<sup>20</sup>

wall of the ground ( $X$ )<sup>2</sup> $\Sigma$  state using the potentials of Pascale gives excellent agreement with the observed emission spectrum. This result, combined with the lack of quenching reported above, justifies the assignment of this emission as arising from the bound–free transition of an isolated Na\*–He exciplex.

The bound levels of the ( $A$ )<sup>2</sup> $\Pi$  state were calculated from the Pascale potential using the BCONT program of LeRoy,<sup>21</sup> which numerically solves the radial Schrödinger equation by use of the Numerov–Cooley algorithm. While the potential supports seven bound states only the first four have been used in calculating the expected bound–free emission spectrum since the contribution from the highest three levels proved to be negligible. The emission lines calculated in the Condon approximation (*i.e.*, constant electronic transition moment), again using the LeRoy program BCONT, are also shown in Fig. 5. We then performed a fit of the observed spectrum, varying only the relative populations of the four vibrational levels. Fig. 5 shows that the agreement between experimental and simulated spectra is excellent, except for the fact that the simulation does not reproduce the small red tail of the observed emission spectrum.

We have performed similar fits to observed emission spectra following excitation from several different wavelengths. In all cases we obtain an excellent simulation of the observed spectrum. Table 2 shows the relative <sup>2</sup> $\Pi$  vibrational populations that result. We see that, as expected, excitation with higher excess energy results in increased population in the higher vibrational levels of the Na\*–He exciplex.

Based upon these observations, we conclude that the red photons arise from emission of Na\* bound to a single He atom. It is less obvious that this species emits from the gas phase, rather than while still bound to the surface of the cluster. In fact, the unassigned red tail of the observed emission can be considered as evidence that a small fraction of the exciplex population remains on the cluster. However, our measurement of an excellent fit with a single decay rate argues that the fraction of exciplexes remaining bound to the He cluster surface is small in the region investigated, in agreement with the spectral fits. Time-resolved studies in the region of the red tail are planned in order to see if the intensity there is due to exciplexes still bound to the cluster surface. Such

**Table 2** Na\*–He vibrational level populations after excitation of Na atoms on He clusters at different energies

	excitation energies/cm <sup>-1</sup>				
	16954.6	16960.7	16975.2	17046.7	17150.7
$v = 0$	0.35	0.33	0.30	0.24	0.10
$v = 1$	0.34	0.34	0.32	0.25	0.22
$v = 2$	0.24	0.25	0.26	0.26	0.27
$v = 3$	0.07	0.08	0.12	0.25	0.41

bound exciplexes would go on to bind further He atoms, effecting a quenching of the observed red fluorescence which would appear in the measured decay.

### (b) Influence of spin–orbit coupling on exciplex formation

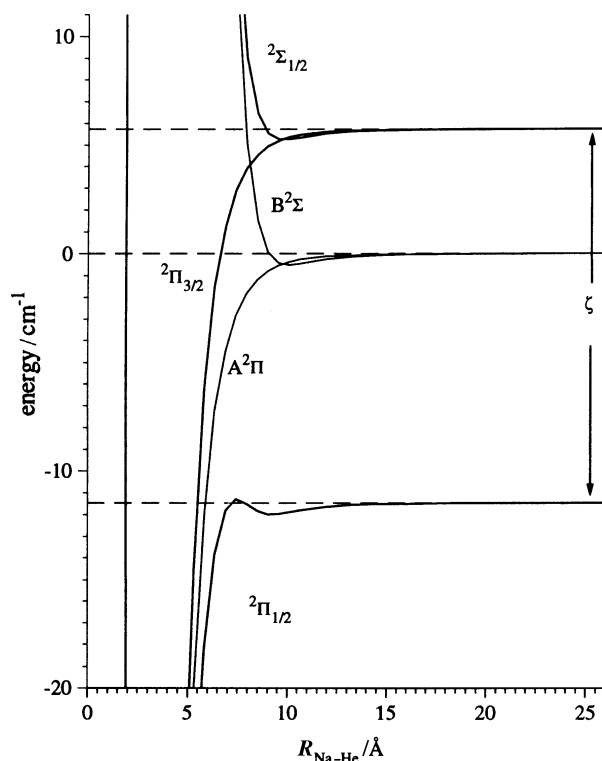
As reported above, we have observed a strong excitation wavelength dependence of the formation rate of the Na\*–He exciplex. At short wavelengths, we observe rapid formation, while at wavelengths to the red of the atomic  $J = 3/2$  transition, we observe a superposition of fast and slow rise times, with the slow rise time becoming dominant at the red extreme of the excitation band. We will now provide a tentative explanation of this phenomenon.

Fig. 6 shows an expanded view of the long range A  $^2\Pi$  and B  $^2\Sigma$  Na–He potentials as calculated by Pascale,<sup>20</sup> using spline interpolation between the *ab initio* points. This calculation, shown as a thin line in the figure, neglects spin–orbit interactions, and thus produces a single  $^2\Pi$  surface. Following Takami and coworkers,<sup>11</sup> we will account for spin–orbit effects by introducing a constant (*i.e.*, independent of the bond length) perturbation equal to the atomic Na  $^2P$  spin–orbit splitting  $\Delta_{so} = 17.19 \text{ cm}^{-1}$ . This should be an excellent approximation at long range, where we expect negligible perturbation of the Na\* electronic structure. In terms of the two potentials  $V_{\Pi}(R)$  and  $V_{\Sigma}(R)$ , the effective Hamiltonian in terms of the basis states [ $^2\Pi_{3/2}$ ,  $^2\Pi_{1/2}$ ,  $^2\Sigma_{1/2}$ ] is:

$$\begin{bmatrix} V_{\Sigma}(x) & \frac{\sqrt{2}}{3} \cdot \Delta_{so} & 0 \\ \frac{\sqrt{2}}{3} \cdot \Delta_{so} & V_{\Pi}(x) - \frac{\Delta_{so}}{3} & 0 \\ 0 & 0 & V_{\Pi}(x) + \frac{\Delta_{so}}{3} \end{bmatrix}$$

We thus see that the spin–orbit operator mixes the  $^2\Pi_{1/2}$  and  $^2\Sigma_{1/2}$  states. Diagonalization of this Hamiltonian for each  $R$  leads to the three curves given in Fig. 6 as thick lines which are labelled by their dominant character at short  $R$ . We thus see that there are two curves, separated at short range by  $2/3$  of the atomic spin–orbit splitting, that correlate with formation of the Na\*–He exciplex. The most natural explanation for our experimental results is that excitation onto the upper,  $^2\Pi_{3/2}$ , surface leads to the rapid formation of the exciplex, while excitation to the lower,  $^2\Pi_{1/2}$ , surface leads to the slow formation of the exciplex.

Notice that unlike the  $^2\Pi_{3/2}$  which is purely attractive at long range, the  $^2\Pi_{1/2}$  surface has a small ‘outer’ well of *ca.*  $0.5 \text{ cm}^{-1}$  at  $R = 9 \text{ \AA}$ , and, centered near  $7.5 \text{ \AA}$ , a small barrier of height  $0.19 \text{ cm}^{-1}$  relative to the  $^2\Pi_{1/2}$  asymptote (although the barrier height relative to the minimum of the outer well is  $0.7 \text{ cm}^{-1}$ ). It is interesting to note that the cluster–Na\* potential (calculated in the frozen cluster approximation and using the sum



**Fig. 6** Long-range view of Na\*–He potentials, neglecting (thin lines) and including (thick lines) the spin–orbit perturbation. Energies are relative to the unperturbed asymptotic value ( $16\,975.8\text{ cm}^{-1}$ )

of two-body potentials) predicts that the cluster–Na\*  ${}^2\Pi$  excited state has a minimum with the Na\* located *ca.* 9 Å above the ‘dimple’ in the He surface.<sup>22</sup> Thus one would expect the closest He atoms to start at a distance from the Na\* close to the outer minimum of the  ${}^2\Pi_{1/2}$  potential. Physically, the barrier on the  ${}^2\Pi_{1/2}$  surface can be understood as arising from the spin–orbit mixing of the  ${}^2\Pi_{1/2}$  and  ${}^2\Sigma_{1/2}$ , as well as from the fact that the Pauli repulsion on the  ${}^2\Sigma_{1/2}$  curve becomes significant at larger distances than the attraction on the  ${}^2\Pi_{1/2}$  surface. A similar barrier in the Ag\*–He exciplex curves was noted by Jakubek and Takami and used to explain the lack of exciplex formation when the  ${}^2P_{1/2}$  level of Ag was excited optically.<sup>23</sup> In that case, however, the barrier was much larger ( $66\text{ cm}^{-1}$ ), as could be expected given the much larger atomic spin–orbit splitting ( $921\text{ cm}^{-1}$ ). The quenching dynamics of the Rb  $D_1$  line in bulk liquid He has also been explained by a barrier due to fine structure along the Rb–He  ${}^2\Pi_{1/2}$  potential surface.<sup>24</sup>

A natural explanation for the slower formation rate for the Na\*–He exciplex on the  ${}^2\Pi_{1/2}$  surface is the presence of this  $0.7\text{ cm}^{-1}$  barrier. While this barrier is very small, it must be remembered that, at the  $T = 0.37\text{ K}$  He cluster temperature,  $kT = 0.25\text{ cm}^{-1}$  and thus a simple classical Boltzmann calculation would predict that a  $0.7\text{ cm}^{-1}$  barrier could reduce the exciplex formation rate by a factor of 16, which would account for the difference in exciplex formation rates observed for the two spin–orbit states. Such a calculation, however, ignores both zero point and tunnelling effects, both of which would be expected to increase the reaction rate.

We have performed a simple semiclassical calculation for the probability that He–Na\* will tunnel through the barrier from the outer well into the inner well by using

the formula:

$$T(E) = \exp\left(-2 \int_{b(E)}^{a(E)} \sqrt{\left\{\frac{2m}{\hbar^2} [U(R) - E]\right\}} dR\right)$$

In the above expression,  $m$  is the reduced mass (3.4 u),  $U(R)$  is the potential of the  ${}^2\Pi_{1/2}$  surface,  $E$  is the energy, and  $a(E)$  and  $b(E)$  are the inner and outer turning points of the barrier. Even if  $E$  is set equal to the energy at the bottom of the outer well (which ignores zero point energy), we estimate a transmission factor  $T = 0.68$ , while for  $E = 0$ ,  $T \approx 1$ . Thus the resultant semiclassical barrier alone is simply too narrow and low to prevent He atoms from rapidly tunnelling through it to form the exciplex. This suggests that the approximation of using the barrier arising solely from the fine structure mixing of the Na\*–He pair potentials and ignoring that the He atom acts in the presence of the whole cluster is insufficient.

It is likely that an accurate modelling of the exciplex formation on the cluster surface will require treatment of the simultaneous interaction of the He with both the Na\* and the rest of the He atoms that make up the cluster. The energy for evaporation of a He atom from a cluster surface is taken to be  $5 \text{ cm}^{-1}$ .<sup>25</sup> Thus the barrier through which the He must tunnel may be thought of as a superposition of the of the He atom–He cluster potential with the NaHe molecular  ${}^2\Pi_{1/2}$  potential. This more complex potential scheme can be seen to increase the height and width of the barrier substantially from that of the simple  $\Pi_{1/2}$  spin–orbit interaction of NaHe. Such a model will also lead to a barrier, albeit smaller, for the formation of the exciplex on the  ${}^2\Pi_{3/2}$  surface.

## Conclusions

This work has demonstrated that the photoinitiated dynamics of impurity species bound to quantum clusters can be studied by the technique of time-correlated single photon counting and describes the apparatus developed for that purpose. As an initial application of this instrument, we have studied the dynamics following the  $3P \leftarrow 3S$  excitation of Na atoms on the surface of helium clusters. We find that emission of desorbed Na\* (collected at  $16980 + 145 \text{ cm}^{-1}$ ) occurs in 50–70 ps, which departs significantly from the ‘instantaneous’ rise ( $\leq 20$  ps) measured in the same apparatus for gas phase Na atoms. This indicates that there is coupling of the excited atom to surface modes of the cluster before desorption and subsequent emission. In the case of hydrogen clusters doped with Na atoms, a rise of *ca.* 20 ps is observed for the emission from the desorbed atom. The dynamics of the Na–(H<sub>2</sub>)<sub>n</sub> coupling, apparently occurring on a faster timescale than in the case of He, are under study at the present time.

Excitation of the  $3P \leftarrow 3S$  transition of Na atoms on He clusters also leads to emission which is red-shifted from the Na ‘D lines’. The rise of this fluorescence collected at  $15800 \pm 125 \text{ cm}^{-1}$  is found to be biexponential. We attribute this to emission from the  ${}^2\Pi_{1/2}$  and  ${}^2\Pi_{3/2}$  potential surfaces of Na\*–He, corresponding to the formation of a free Na\*–He exciplex as verified by successful simulation of frequency-resolved dispersed emission spectra. While excitation along the  ${}^2\Pi_{3/2}$  surface of Na\*–He yields fluorescence with a rise time equivalent to that of the desorbed Na\* atoms (*ca.* 70 ps), emission from the  ${}^2\Pi_{1/2}$  surface exhibits a 700 ps rise.

The large difference in exciplex formation rate with spin–orbit state represents the most unexpected observation of this work. Including spin–orbit effects in the NaHe *ab initio* potentials of Pascale<sup>20</sup> gives rise to a small ( $0.7 \text{ cm}^{-1}$ ) barrier on the  ${}^2\Pi_{1/2}$  potential surface due to the need to partially decouple from the more repulsive  ${}^2\Sigma_{1/2}$  state. However, we determine that this barrier has too limited an opacity to significantly impede tunnelling of the He atom into the potential well of the lower  ${}^2\Pi$  state of NaHe. We suggest that the energy required to extract the He atom from the cluster must be

taken into account in order to reproduce the dynamic effects that we have found to occur in exciplex formation.

The authors would like to thank Professor Warren Warren for use of laser equipment, Donna Strickland, John Eng, and Matthew Radcliff for assistance in some of the experiments, and the AFOSR (HEDM Program) Contract: F49620-95-1-0086.P0001 for financial support.

## References

- 1 J. H. M. Beijersbergen, Q. Hui and M. Takami, *Phys. Lett. A*, 1993, **181**, 393.
- 2 A. Fujisaki, K. Sano, T. Kinoshita and T. Yabuzaki, *Phys. Rev. Lett.*, 1993, **71**, 1039.
- 3 T. Yabuzaki, T. Kinoshita, K. Fukuda and Y. Takahashi, *Z. Phys. B*, 1995, **98**, 387.
- 4 T. Kinoshita, Y. Takahashi and T. Yabuzaki, *Phys. Rev. B*, 1994, **49**, 3648.
- 5 T. Kinoshita, K. Fukuda and T. Yabuzaki, *Phys. Rev. B*, 1996, **54**, 6600.
- 6 S. Kanorsky, A. Weis, M. Arndt, R. Dziewior and T. W. Hänych, *Z. Phys. B*, 1995, **98**, 371.
- 7 J. Dupont-Roc, *Z. Phys. B*, 1995, **98**, 383.
- 8 T. Kinoshita, K. Fukuda, T. Matsuura and T. Yabuzaki, *Phys. Rev. A*, 1996, **53**, 4054.
- 9 F. Ancilotto, E. Cheng, M. W. Cole and F. Toigo, *Z. Phys. B*, 1995, **98**, 323.
- 10 F. Stienkemeier, J. Higgins, C. Callegari, S. I. Kanorsky, W. E. Ernst and G. Scoles, *Z. Phys. D*, 1996, **38**, 253.
- 11 J. L. Persson, Q. Hui, Z. J. Jakubek, M. Nakamura and M. Takami, *Phys. Rev. Lett.*, 1996, **76**, 1501.
- 12 T. E. Gough, M. Menge, P. A. Rowntree and G. Scoles, *J. Chem. Phys.*, 1985, **83**, 4958.
- 13 D. V. O'Connor and D. Phillips, *Time-correlated Single Photon Counting*, Academic Press, San Diego, 1984.
- 14 Hamamatsu Technical Service Notes, 1987.
- 15 P. R. Bevington and D. K. Robinson, *Data Reduction and Error Analysis for the Physical Sciences*, McGraw-Hill, New York, 1992.
- 16 A. A. Radzig and B. M. Smirnov, *Reference Data on Atoms, Molecules, and Ions*, Springer-Verlag, New York, 1985.
- 17 S. Cova, M. Ghioni and F. Zappa, *Rev. Sci. Instrum.*, 1991, **62**, 2596.
- 18 C. Callegari, J. Higgins, F. Stienkemeier and G. Scoles, *J. Phys. Chem. A*, 1998, **102**, 95.
- 19 M. D. Havey, S. E. Frolking and J. J. Wright, *Phys. Rev. Lett.*, 1980, **45**, 1783.
- 20 J. Pascale, *Technical Report, Service de Physique des Atoms et des Surfaces*, 1991 (C. E. N. Saclay, Gif sur Yvette-Cédex, France).
- 21 R. J. LeRoy, *Comput. Phys. Commun.*, 1989, **52**, 383.
- 22 S. I. Kanorsky, personal communication.
- 23 Z. Jakubek and M. Takami, *Chem. Phys. Lett.*, 1997, **265**, 653.
- 24 T. Kinoshita, K. Fukuda, T. Matsuura and T. Yabuzaki, *Phys. Rev. A*, 1996, **53**, 4054.
- 25 S. Stringari and J. Treiner, *J. Chem. Phys.*, 1987, **87**, 5021.